HYDROLOGICAL PROCESSES
Hydrol. Process. (2013)
Published online in Wiley Online Library
(wileyonlinelibrary.com) DOI: 10.1002/hyp.9867

Storage dynamics simulations in prairie wetland hydrology models: evaluation and parameterization

Kevin Shook,[1]* John W. Pomeroy,[1] Christopher Spence[2] and Lyle Boychuk[3]

[1] *Centre for Hydrology, University of Saskatchewan, Saskatoon S7N 5C8, Canada*
[2] *National Hydrology Research Centre, 11 Innovation Boulevard, Saskatoon SK S7N 3H5, Canada*
[3] *Ducks Unlimited Canada, P.O. Box 1030 Winnipeg St., Regina, SK, S4R 8P8, Canada*

Abstract:

The contributing areas of streams in the Prairie regions of Canada and the northern U.S. are dominated by complexes of wetlands which store and release water. Prior research has suggested the existence of hysteresis between the total volume of water stored in prairie wetlands within a drainage basin and the basin's contributing area. To simulate the relationship between storage and contributing area in a way that accounts for hysteresis, two wetland hydrology models with vastly different levels of complexity were devised.

The fully distributed Wetland Digital Elevation Model (DEM) Ponding Model (WDPM) applies simple fluxes of runoff and evaporation to a DEM of a prairie wetland complex. The parameterized Pothole Cascade Model (PCM) applies simulated fluxes of water to collections of conceptual models of wetlands and is less demanding in computations and data. Prior research showed that both models produced hysteretic relationships between water storage and contributing area, but the PCM produced smaller estimates of contributing area than did the WDPM, likely due to its spatial simplification.

Using sequential remote sensing observations of wetland area after snowmelt, this study shows that the frequency distribution of the open water areas of prairie wetlands is similar to that produced by the WDPM when the wetlands are close to being completely filled. The remotely sensed observations show evidence of hysteresis in the open water area frequency distributions, as predicted by the fully distributed WDPM. To enable the parameterized PCM to produce the same type of hysteretic relationships as the WDPM, scaling relationships between the maximum area of a wetland and the area of upland draining into it were included. The parameterized PCM is suitable for application with prairie snow redistribution, snowmelt, infiltration, runoff and evapotranspiration routines as part of semi-distributed hydrological modelling of prairie wetland basins such as that implemented in the Cold Regions Hydrological Model. Copyright © 2013 John Wiley & Sons, Ltd.

KEY WORDS wetland hydrology; variable contributing area; depressional storage; Canadian Prairies; distributed modelling; hysteresis; remote sensing

Received 15 October 2012; Accepted 22 April 2013

INTRODUCTION

The hydrology of the formerly glaciated Prairie region of Canada and the northern United States is quite distinctive because of the dominance of snowmelt runoff events in generating streamflow, the lack of baseflow from groundwater discharge and the extreme inter-seasonal and inter-annual variability in streamflow which is partly due to high variability in streamflow response to snowmelt or rainfall–runoff inputs and partly due to high climatic variability (Fang and Pomeroy, 2007; Pomeroy *et al*., 2007a). The climate is cold and semi-arid to sub-humid with the majority of runoff occurring over a few weeks when the melt rate of the wind redistributed seasonal snowpack exceeds the infiltration rate to frozen soils (Gray *et al*., 1989). Summer rains are intermittent, but can occasionally have sufficient intensities to cause runoff over small areas (Elliott and Efetha, 1999; Shook and Pomeroy, 2012). Interflow and groundwater discharge are normally negligible, soils are normally unsaturated, and rainfall is normally insufficient to sustain summer streamflow (Fang *et al*., 2010; Pomeroy *et al*., 2010), though there can be important exceptions to this in extremely wet years.

The hydrography of the Prairies is also unusual. The topography is comparatively flat, and of glacial and post-glacial origin with many features such as moraines, flutings, drumlins, outwash plains, glacial outburst valleys, sand dunes and glacially dammed lake beds that are due to the ice age conditions of the Pleistocene (Christiansen, 1979). Since glaciation, the region has primarily sustained arid to sub-humid climates, consequently there is not sufficient runoff, energy or time for fluvial erosion to develop the drainage systems familiar in more temperate regions. Much of the Prairies are internally drained to small 'prairie pothole' wetlands that are a relic of remnant pieces of glacial ice. These wetlands percolate to groundwater very slowly due to low permeability subsurface glacial till and so only have outflows when their storage capacity is exceeded (van der Kamp and Hayashi, 1998).

*Correspondence to: Kevin Shook, Centre for Hydrology, University of Saskatchewan, Saskatoon S7N 5C8, Canada.
E-mail: kevin.shook@usask.ca

Shaw *et al.* (2011) investigated and modelled the wetland surface runoff generation process after comparable hillslope scale processes identified by Spence and Woo (2003) (who originated the term 'fill and spill') and Tromp-van Meerveld and McDonnell (2006). Because there can be long periods without spilling, large parts of the region have been designated as being 'non-contributing' to local streams by Agriculture and Agri-Food Canada (AAFC) (Godwin and Martin, 1975), based on the definition of contributing to streamflow with an annual probability of 0.5 or smaller. In reality, the non-contributing areas of basins in the region are dynamic and change with the amount of water in depressional storage (Stichling and Blackwell, 1957; Gray, 1964; Pomeroy *et al.*, 2010; Shaw *et al.*, 2011). The dynamic nature of the contributing area invalidates all conventional hydrological models which require a basin's contributing area to be a fixed value.

The designated non-contributing region for streams which drain into Canadian rivers is plotted in Figure 1 using data obtained from AAFC (http://www. rural-gc.agr.ca/pfra/gis/gwshed_e.htm). Figure 1 also demonstrates that the extent of the designated non-contributing region generally coincides with that of the Canadian Prairie ecozone as defined by Marshall *et al.* (1996). The largest rivers within the ecozone are exotic, being sourced primarily from the Canadian Rockies and the foothills to the west (Pomeroy *et al.*, 2007b). Of the uncontrolled basins having gauged outlets within the ecozone and with gross areas smaller than 1000 km^2, the total effective contributing area (10 846 km^2) is approximately 61% of the total gross area of the basins (17 879 km^2).

As depressions fill, they connect and allow water to travel to a stream. Conversely, as the depressions empty, their interconnections break, reducing the contributing area. Modelling the state of depressional storage, and therefore the contributing area, is complicated by the diversity of depressions, which range from puddles to permanent wetlands. Kuchment *et al.* (2000) postulated that the surface depressional storage of the upper Kolyma River basin in the permafrost region of Russia could be represented by a continuous exponential distribution (f) of the form

$$f(P) = \frac{1}{\hat{P}} \exp\left(-\frac{P}{\hat{P}}\right), \quad (1)$$

where P is the maximum possible depressional storage, and $\hat{P}$ is a given depressional storage.

Assuming that the depressional storages are filled in order of increasing size, the total storage (D) can be computed by integrating f(P). The initial value of the total storage before the melt was assumed to be related to the antecedent precipitation.

Although the method of Kuchment *et al.* (2000) does provide for a distribution of depressional storage, its methods of filling and emptying the storage are not valid on the northern Prairies. Water is added to prairie wetlands through direct precipitation, by deposition of wind redistributed snow that melts *in situ*, by runoff of rainfall and melting snow from the local catchment area, from streamflow into the wetland, and from the spill of, and subsequent runoff from, upstream wetlands (Fang and Pomeroy, 2008). Water is removed from wetlands by open water evaporation, evapotranspiration via wetland and riparian vegetation, downstream drainage, infiltration to soils and percolation to groundwater (Hayashi *et al.*, 2003). As prairie wetlands are not arranged in a simple sequence, the assumption that depressional storages are filled or emptied in size order is likely not to be valid and calls into question the applicability of Equation (1) in the Canadian Prairies.

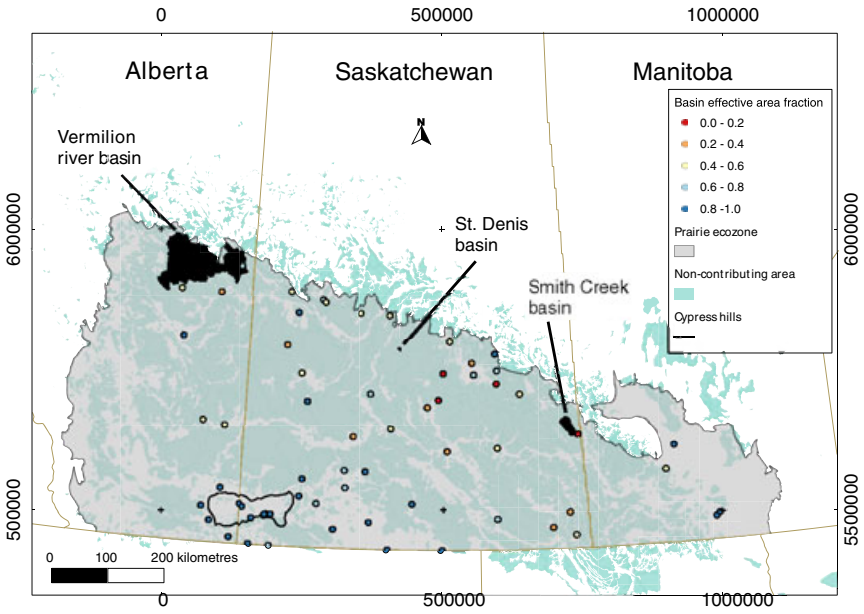

Figure 1. Locations of the Vermilion, St. Denis and Smith Creek basins in Western Canada. The location of the prairie ecozone and the extent of the 'non-contributing' areas of rivers draining into Canada are also plotted. Projection is UTM 13

DOI: 10.1002/hyp

Further, the various fluxes of water entering and leaving a wetland have differing contributing areas. Fang and Pomeroy (2008) show varying contribution area for individual wetlands, and Shook and Pomeroy (2011) theorized that differences in the contributing areas of individual wetlands for filling and emptying fluxes cause hysteresis in the relationship between depressional storage and contributing area at the basin scale. Therefore, no single-valued function, such as Equation (1), can describe the contributing area of a wetland-dominated prairie basin as a function of basin-wide water storage alone; the spatial distribution of water storage must also be known.

Hysteresis is also found in other types of post-glacial basins which are dominated by depressional storage. Spence *et al.* (2010) and Phillips *et al.* (2011) found evidence of hysteretic relationships between water storage and streamflow in Baker Creek research catchment in the subarctic Canadian Shield of the Northwest Territories. Similar hysteretic relationships were also found by Oswald *et al.* (2011) for a basin in the boreal Canadian Shield in northwestern Ontario. As with the Prairies, the Canadian Shield is a region of low relief, where the water storages exhibit thresholds. Unlike the Prairies, the Canadian Shield is dominated by bedrock, its forests prevent snow redistribution to lakes and it has large interconnected lakes rather than small generally isolated wetlands, so the hysteresis effects exhibited by basins in the two regions may be different. It is not known whether the Russian landscapes modelled by Kuchment *et al.* (2000) have wetlands that display hysteresis – most of Russia was deglaciated much earlier than most of Canada and subsequently was subject to a more humid climate where fluvial erosion processes could contribute to the development of drainage networks. It is the lack of fluvial geomorphology in much of Canada that leads not only to high depressional storage, but to some sort of hysteresis in storage and contributing area relationships.

The existence of hysteresis between storage and contributing area in the Prairies requires explicit modelling of the changes in contributing area in hydrological models of a wetland-dominated prairie basin. The authors have developed two models which are capable of simulating hysteresis in calculating the dynamic nature of contributing area in prairie wetland complexes: the fully spatially distributed Wetland Digital Elevation Model (DEM) Ponding Model (WDPM) and the parameterized Pothole Cascade Model (PCM) (Shook and Pomeroy, 2011).

These programs were developed to test methods for representing prairie wetlands in hydrological simulations of the prairie pothole region. They are models in that they are simplified representations of complex phenomena. They are not intended to act as complete simulations of all hydrological processes in the region, but to act as components performing internal routing of water within a hydrological simulation.

It is also important to note that the models are hydraulic, rather than hydrological. As the models are not intended to represent the complex hydrological processes of the region, it is not currently feasible to compare simulated outputs (discharges) against measured discharges. However, the intent of this research is to test the abilities of the models to reproduce the observed state variable of open water (depressional storage) area within a region, and the relationships between the state variable and contributing area. As will be demonstrated, these variables and relationships can be tested and validated without the use of streamflow.

The WDPM models the destination of liquid water applied to a fine-scale DEM of a wetland-dominated prairie landscape. The WDPM requires high-resolution DEMs such as those produced from airborne LiDAR measurements (Minke *et al.*, 2010) and models the storage and runoff formation from complexes of many thousands of wetlands. It is expensive computationally and demanding in its information requirements.

The PCM models the application and removal of water from individual wetlands and is therefore amenable to parameterization by application to conceptual formulations of wetland distributions. The PCM is easier to adopt than is the WDPM in current prairie semi-distributed models in Canada that are based on land surface tiles or hydrological response units such as Modelization Environmentaire Surface and Hydrology (Mekonnen *et al.*, (n.d.)) and Cold Regions Hydrological Modelling Platform (CRHM; Pomeroy *et al.*, 2007a, b).

The objective of this research is therefore to make an advance toward the development of a general physically based model of the hydrology of prairie wetland dominated drainage basins by evaluating a fully spatially distributed calculation of wetland hydrology with observations of storage and then parameterizing a more conceptual model with results of the more detailed model.

The intent is to contribute to the development of a hydrological model where physically based calculations of hydrological fluxes will result in accurate simulations of the interrelated dynamics of wetland water storage, contributing area and the translation of runoff to streamflow generation on a basin scale.

RESEARCH BASINS

Research was carried out using detailed spatial topographic data from three basins in Alberta and Saskatchewan, Canada: Smith Creek Research Basin (SCRB) in the Assiniboine River Basin of eastern Saskatchewan, St. Denis Basin and National Wildlife Area in the South Saskatchewan River Basin of south-central Saskatchewan and the Vermilion River Basin of the North Saskatchewan River Basin of east-central Alberta. These basins were selected because LiDAR DEM data were available – conventional DEM data cannot accurately represent drainage networks, wetland locations and depressional storage in this region (Fang *et al.*, 2010). Additional high-resolution satellite data were available for SCRB and St. Denis Basin. The locations of the three basins are mapped in Figure 1.

DOI: 10.1002/hyp

SCRB

SCRB has a gross area of 445 km^2. The basin has very mild topography, such that it is difficult to determine overland flow directions from photogrammetrically derived elevations. It contains a stream which normally flows for a few weeks each spring in response to snowmelt runoff. This basin has been studied by the University of Saskatchewan Centre for Hydrology since 2007 (Fang *et al*., 2010; Minke *et al*., 2010; Pomeroy *et al*., 2010; Shook and Pomeroy, 2011; Brunet and Westbrook, 2012). LiDAR data were acquired from October 14 to 16, 2008 at a horizontal resolution of 1 m, with a vertical RMS error of 0.05 m. The collection procedure is documented more fully by Lidar Services International (2009). The 1 m data were resampled to a DEM with a resolution of 10 m for ease of use. Using the LiDAR-based DEM, SCRB was divided into five sub-basins by Fang *et al*. (2010) using TOPAZ (Garbrecht and Martz, 1997) software to determine drainage areas and stream channel locations (Figure 2). Because some of the wetland analyses were computationally intensive, they were restricted to sub-basin 5 which has an area of 12 km^2. At a resolution of 10 m, the sub-basin 5 DEM, which was used for modelling, measured 482 $\times$ 471 elements (10 m $\times$ 10 m), the number of elements inside the sub-basin being reduced by its irregular boundary.

A RapidEye satellite image of the region captured on May 18, 2011 with a pixel size of 5 m was made available by Ducks Unlimited Canada. RapidEye is a constellation of five Earth Observation satellites which sense spectral bands of blue (440–510 nm), green (520–590 nm), red (630–685 nm), red edge (690–730 nm) and near-infrared (NIR) (760–850 nm) radiation.

The image was classified into water and water-free regions by developing a binary mask using the RapidEye NIR channel, which is strongly absorbed by water, (Lillesand *et al*., 2004). An upper threshold was applied to the NIR data, with the thresholded values providing the mask. The value of the threshold was determined iteratively by checking the resulting mask against LiDAR DEM data and oblique aerial photos collected a week prior to the RapidEye image. Förster *et al*. (2010) demonstrated the ability of automatically classified multi-temporal RapidEye images to consistently discriminate between open water and other landscapes.

On the Prairies, the difficulty in determining the water edge by remote sensing can be increased by a 'willow ring' of tall vegetation (brush or trees) which often surrounds a wetland (Hayashi *et al*., 1998), and which can shield the water from direct observation in solar radiation wavelengths. Due to the extreme wetness of SCRB in the spring of 2011, most of the wetlands were flooded outside of their willow rings, making it relatively easy to discriminate between the water and the surrounding uplands using the RapidEye images.

St. Denis Basin and National Wildlife Area

The St. Denis Basin is located approximately 20 km east of Saskatoon, SK, and has an area of 11 km^2. The region has quite high relief for a prairie landscape, being composed of moderately rolling knob-and-kettle moraine with some slopes of up to 10 to 15% (van der Kamp *et al*., 2003). The connectivity of the wetlands in this basin has been studied extensively (Shaw, 2009; Shaw *et al*., 2011) as has wetland basin wind redistribution of snow and snowmelt hydrology (Fang and Pomeroy, 2008, 2009) and evapotranspiration (Armstrong *et al*., 2008). The basin does not have a well-defined stream channel, although Shaw *et al*. (2011) found evidence of a disconnected network and that wetlands can episodically join together via an ephemeral channel, spilling to a terminal pond, as shown in Figure 3 (Spence, 2007).

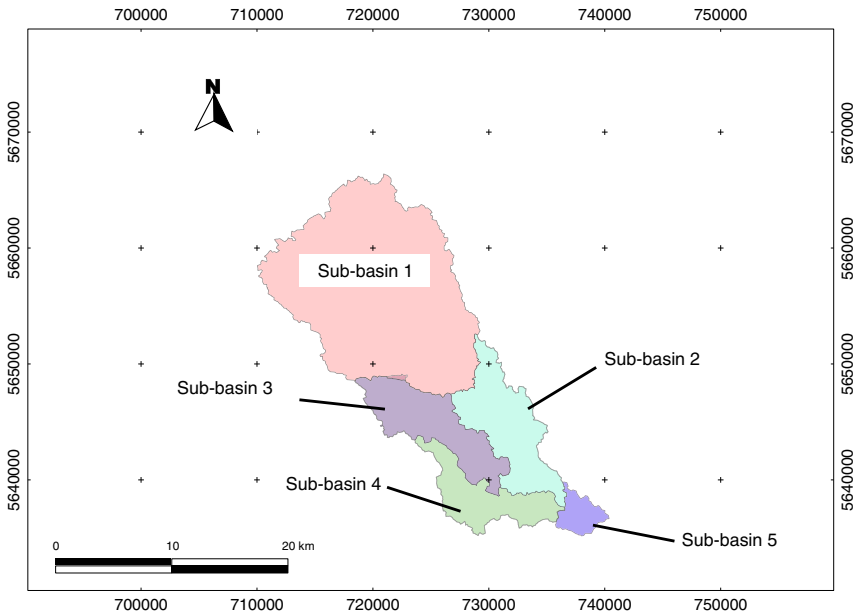

Figure 2. Arrangement of sub-basins within the SCRB. LiDAR coverage exists for the entire basin. Projection is UTM 13

DOI: 10.1002/hyp

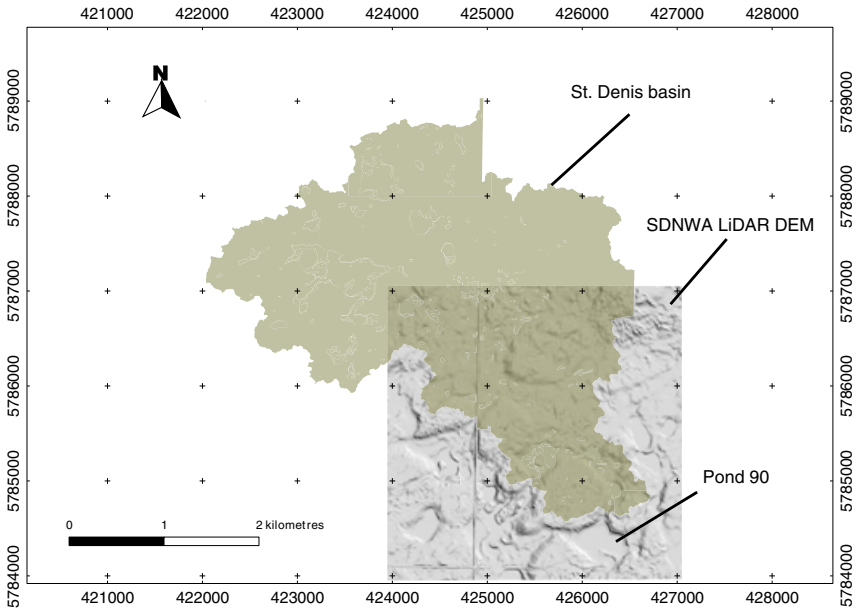

Figure 3. St. Denis Basin and LiDAR coverage of St. Denis National Wildlife Area. Projection is UTM 13

Much of the basin is located inside the St. Denis National Wildlife Area (SDNWA), as shown in Figure 3. Environment Canada has recorded wetland levels at SDNWA since 1968, and the site has been studied intensively by researchers based at the University of Saskatchewan since 1980 (Driver and Peden (1977), Miller *et al*. (1985), van der Kamp *et al*. (2003), Shaw (2009)). LiDAR data were collected on SDNWA on August 9, 2005, with a vertical resolution of 0.2 m and a horizontal resolution of 0.5 m, although this research used an integrated version with a horizontal resolution of 6 m (Töyrä, 2005). At this resolution, the LiDAR DEM measures 512 × 512 elements (6 × 6 m).

Observations of the stream network at St. Denis were made on foot and by truck throughout the period of streamflow during the spring and summer of 2011. These observations were used to ground truth SPOT 5 10 m resolution multispectral satellite imagery obtained on April 13, April 30, May 13 and July 21, 2011. The images were atmospherically corrected and orthorectified with eight ground control points to a 1 m resolution LiDAR image collected using methods summarized by Fang and Pomeroy (2009). The images were classified into ice, ponded water, saturated and unsaturated classes with a supervised maximum likelihood classifier with the four multispectral bands and the modified normalized difference water index (Xu, 2006) used as inputs. Classification accuracy was 98.3%, and the kappa coefficient of the classification (Congalton, 1991) was 0.98 compared to field observations.

Vermilion River Basin

The Vermilion River Basin is located in east-central Alberta and has a gross basin area of 7860 km^2. As part of a research project carried out by the Centre For Hydrology (Pomeroy *et al*., 2012), a LiDAR DEM measuring 660 × 665 elements (each element measuring 15 × 15 m) was acquired, giving a total area of 98.7 km^2. Of this DEM, an area of about 95 km^2 was within the basin and was used for analyses, as shown in Figure 4. The LiDAR DEM was obtained through AltaLIS, and it has a stated horizontal accuracy of 50 cm and a vertical resolution of 30 cm. No high-resolution remotely sensed measurements of open water areas were available for this site.

METHODOLOGY

The WDPM

The WDPM is a fully distributed model of wetland storage and runoff that was described in Shook and Pomeroy (2011), where it was denoted as Model 1. It is not a full hydrological model, but simply a model of depressional storage filling and depleting. The model finds the final spatial distribution of excess precipitation (water) evenly applied over a LiDAR-based DEM, using the iterative algorithm of Shapiro and Westervelt (1992). The WDPM is difficult to use as the basis for a basin-scale hydrological model as it assumes uniform precipitation inputs which are inconsistent with wind redistribution of snow to depressions (Pomeroy *et al*., 1993; Fang and Pomeroy, 2009), uniform open water evaporation losses which are inconsistent with enhanced advection of energy to and consequently enhanced evaporation from small water bodies (Granger and Hedstrom, 2011) and it is very slow to run. For example, the WDPM typically took over 16 h (using a 3.06 GHz Intel Xeon 64-bit processor) to model the distribution of a single application of water to a precision of 1 mm, over the relatively small DEM of SCRB sub-basin 5. This slowness is despite the model's physics being intentionally simplified; the WDPM does not represent the

DOI: 10.1002/hyp

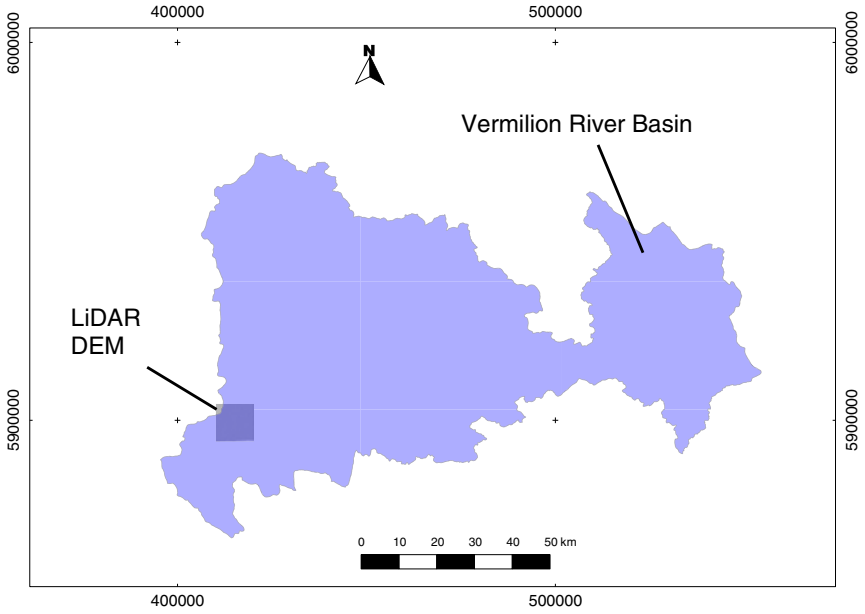

Figure 4. Vermilion River basin and LiDAR coverage. Projection is UTM 13

temporal variability of storage and flow as it does not incorporate a time step, nor does it include the full range of processes that lead to wetland filling and depleting. Improving the physics of the model with a full suite of processes (snow redistribution, melt, runoff, evaporation) would require fully spatially distributed simulation of the spring freshet, and many alternating cycles of rainfall and evaporation to capture the hysteresis amongst wetland water storage and wetland open water area and contributing area (Shook and Pomeroy, 2011). Given a sufficiently large basin and a wet year (with many intermittent rain events), it is possible that the WDPM could not be executed in real time.

There are other limitations to this model. Because the DEM is based on LiDAR, the model cannot simulate depressional storage water elevations below those which were present at the time when the LiDAR was collected. The horizontal resolution of the LiDAR datasets limits the minimum size of wetlands and water areas that can be modelled. Despite its potential shortcomings, the WDPM is the most detailed model of a network of fill and spill depressional storage that has been devised and is considered likely to correctly represent the filling and subsequent draining of wetlands under a wide range of circumstances.

The PCM

The PCM, is a more conceptual wetland model than the WDPM and was described in Shook and Pomeroy (2011) where it was denoted as Model 2. The PCM is based on the work of Shaw (2009) in that it simulates the filling and spilling of a set of prairie wetlands which are modelled as discrete reservoirs. The PCM differs from Shaw's model in that it uses much larger numbers of wetlands, and the areas of modelled wetlands are statistically representative of the areas of wetlands in a basin. The connectivity of the modelled wetlands is also statistically representative of that of wetlands in a basin. The code of the PCM is unrelated to Shaw's. The advantage of the PCM, as compared to the WDPM, is that it is computationally efficient, requiring a few seconds to complete simulations that would take hours with the WDPM.

Because of its speed and spatial simplicity, the modelled wetlands in the PCM can be forced with physically based calculations of the water fluxes into and out of the wetlands (direct precipitation, blowing snow redistribution, snowmelt runoff, rainfall and evaporation) using a physically based model such as CRHM (Pomeroy *et al*., 2007a, b; Fang *et al*., 2010), or by the simple additions and removals of water as with the WDPM. Unlike the WDPM, the model wetlands of the PCM are not restricted by the resolution of a DEM, and they can model any depth of water. The simplified spatial structure of PCM permits it to more realistically parameterize the outputs from the wetland via evaporative loss. As discussed previously, Prairie wetlands are often surrounded by a riparian 'willow ring' of trees and shrubs which is submerged in wet years and whose roots can draw water from the wetland in dry years. As the willow ring is well-watered, its evapotranspiration rates are similar to those of a free-water surface and can be much higher than the rates from surrounding semi-arid landscape. Therefore, the effective area of evapotranspiration from the wetland is greater than would be expected from the Hayashi and van der Kamp (2000) relationships, when the water surface area is smaller than that of the willow ring. This effect is included in the PCM.

As was noted by Minke *et al*. (2010), real wetland shapes and frequency distributions have fractal characteristics. The PCM wetland shapes are based on the work of Hayashi and van der Kamp (2000), who developed simple equations to describe the relationships amongst

DOI: 10.1002/hyp

water depth, surface area and volume for prairie wetlands. The PCM derives its model wetland dimensions from a random selection of the frequency distributions of wetland maximum water areas and volumes for a given basin. These values were determined from LiDAR data, using volume–area–depth scaling and DEM infilling techniques described by Fang *et al.* (2010). PCM therefore simulates wetlands as Euclidean objects that can only approximate the behaviour of real wetlands and so the wetland storage capacities and drainage network require parameterization to be able to simulate real wetland drainage basin hydrological behaviour.

Unlike real wetlands or WDPM-modelled wetlands, the PCM conceptual wetlands are unable to subdivide when water levels decline below internal sill elevations. Thus, when the wetlands are not completely full, PCM cannot accurately simulate the number of wetlands, their size and consequently their frequency distribution. This is not expected to have important consequences for water balance calculations, such as the evapotranspiration loss, but will for runoff calculations.

RESULTS

Fitting frequency distributions to remotely sensed open water areas

Zhang *et al.* (2009) found that open water areas in North Dakota could be described well by simple power-law relationships between the number of lakes of a given size and the class size. The power laws, which plot as straight lines on logarithmic graphs, were found to fit well over scales between 100 and 30 000 m^2 and between 6000 and 100 000 m^2. The power-law distribution used by Zhang *et al.* (2009) is a version of the Pareto distribution. Data that fit a Pareto distribution also plot as a straight line against their exceedance probabilities on a logarithmic graph. The cumulative distribution of the Generalized Pareto Distribution (GPD) is defined as (Coles, 2001)

$$F(z) = GDP(\mu, \sigma, \xi) = 1 - \left[1 + \xi\left(\frac{z-\mu}{\sigma}\right)^{-1/\xi}\right], \quad (2)$$

where μ is the location parameter, σ the scale parameter and ξ the shape parameter ($\xi \neq 0$).

A separate GPD was fitted to each of the sets of open water areas determined from the classified remotely sensed images of the St. Denis and Smith Creek basins, using the Open Source statistical language R (R Development Core Team, 2011). The distributions were fitted by the method of Maximum Likelihood Estimation (Ricci, 2005). The null hypotheses, which the fitted distributions described the frequencies of the remotely sensed water areas, were accepted at a 5% level in all cases, using Chi-squared tests.

Deviation of water area frequency distributions from power laws. Although the distributions of the remotely sensed open water areas were statistically well-described by the GPD, it does not follow that the GPD is always useful to describe the details of a particular frequency distribution. For example, the logarithmic plots of Zhang *et al.* (2009) show some divergence from linearity, particularly for the smallest areas. Similarly, Seekell and Pace (2011) noted that the areas of lakes in Wisconsin and New York diverged from simple Pareto distributions. They found that the divergence from linearity was caused by the underlying frequency distribution deviating from the ideal Pareto distribution, rather than being an artifact of undersampling.

Figure 5 plots the resulting frequency distribution of wetland/lake open water areas at Smith Creek determined from the RapidEye image as described. These data were selected for analysis because the very large number of wetlands provides the most conclusive test of whether the apparent deviations of the water area frequency distribution plots from simple power laws is due to undersampling. The exceedance frequencies of approximately 85 000 open water areas, ranging in size from 25 m^2 to 2.6 million m^2, are plotted. The exceedance frequencies were determined using the empirical cumulative distribution function in R, which was used for all subsequent frequency estimations in this research (Ricci, 2005). The large number of wetlands and the large area covered demonstrates that the curvature in Fig. 5, indicative of a deviation from the power-law distribution, is found over a wide range of scales. As the scales of curvature far exceed the minimum resolution of the remote sensing, the curvature is not likely due to undersampling of the lower tail of the distribution.

To assess models other than a simple power law, least-squares regression models of the log-transformed open water areas and exceedance probabilities were determined for linear, second- and third-order polynomials, which are plotted, respectively, as black, red and blue curves, in Figure 5. The values of r^2 for the linear, second-order and third-order polynomial models were 0.915, 0.998 and 0.999, respectively. The large value of the correlation

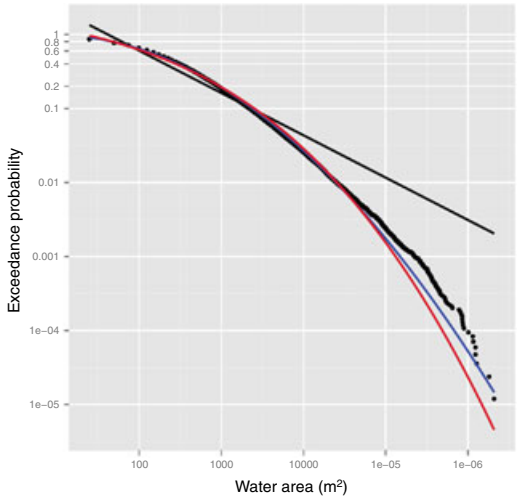

Figure 5. Logarithmic plot of exceedance probability *versus* area for water remotely sensed at SCRB on May 18, 2011. The black, blue and red lines represent linear, second- and third-order polynomials, respectively, fitted to the log-transformed probabilities and areas

DOI: 10.1002/hyp

coefficient for the linear model is greater than might be expected from a visual examination of the plot, due to the presence of large numbers of identically sized, small open water areas, that are fitted much better than are the few large values. The two polynomial models produced better values for r^2 than did the linear model, and they better described the evident departure of the frequency distribution from a simple power law. Because of the small difference between the second- and third-order correlation coefficients, second-order polynomials, which have fewer coefficients, are fitted to all subsequent log-transformed distributions.

Temporal changes in water area frequency distributions at SDNWA. Zhang *et al.* (2009) plotted frequency distributions of open water areas over the period 1990–2002. Unfortunately, the distributions were separated in time by months or years, making it difficult to isolate the effects of antecedent precipitation, runoff and evaporative loss on the distributions of open water areas. By contrast, the remotely sensed data from the St. Denis Basin were collected at much more frequent intervals and can be compared to local records of precipitation and runoff.

Figure 6 plots frequency distributions of open water areas estimated by remote sensing at St. Denis Basin on April 13, 30 and May 13, 2011, together with second-order polynomials fitted to the points. The total open water area as a percentage of the basin area and the coefficients of the polynomials are listed in Table I.

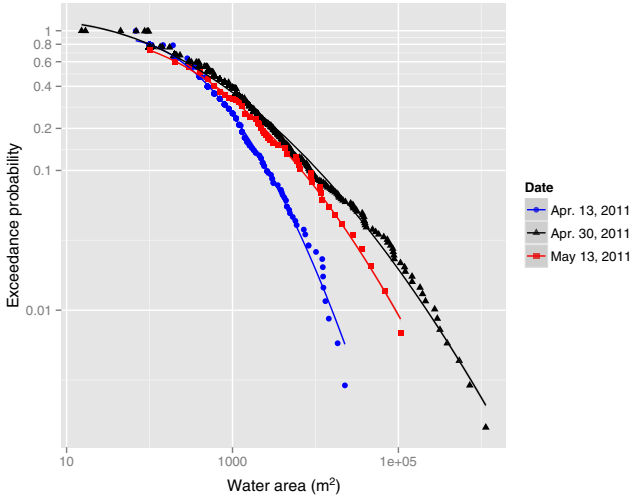

Figure 6. Logarithmic plot of exceedance probability *versus* area for water remotely sensed at St. Denis Basin on April 13, April 30 and May 13, 2011. The lines represent second-order polynomials fitted to the log-transformed probabilities and areas

The percentage of water increased from 4.4% on April 13 to 11.9% on April 30 due to the spring snowmelt freshet, which is one of the few types of prairie hydrological events capable of causing surface runoff (Gray *et al.*, 1986). The total fractional open water area decreased to 7.5% on May 13, 2011. As 14.1 mm of precipitation fell over this period at SDNWA, the decrease in open water area must have been be due to the sum of evaporation, infiltration and natural drainage exceeding the sum of direct precipitation and runoff from rainfall and snowmelt.

Over the interval April 13 – 30, the frequency distribution plot of open water areas in Figure 6 appears to pivot counter-clockwise, which is borne out by the large changes in the magnitudes of the intercepts, linear and quadratic coefficients of the fitted polynomials. Over the interval April 30 – May 13, the plot shifted leftward, as shown by the comparatively large change in the magnitude and sign of the polynomial intercepts, although it is difficult to see in the figure. The smaller change in the linear coefficient indicates a clockwise rotation, while the quadratic coefficient showed the smallest change.

By July 21, 2011, the total open water area had declined to 4.5% of the basin area. Although the total area of open water was nearly identical to that measured on April 13, the frequency distributions of open water areas on the two dates are very different, as shown by the plots in Figure 7. The polynomial coefficients listed in Table I show that the intercept coefficient had the greatest change in magnitude over the period May 13 – July 21. Over this interval, 186.6 mm of rain was measured at the SDNWA rain gauge. Runoff from this rainfall and direct inputs of rain must have been exceeded by evaporation, draining and wetland-focused recharge to cause the observed reduction in water area and therefore depressional storage. The different observed probability distributions of open water areas of wetlands for similar total water areas confirm the existence of hysteresis in the filling and emptying of prairie wetland complexes. Very different states of individual wetland areas were manifested by very similar total open water areas. Figure 7 also demonstrates that the areas of the largest water bodies are very similar on April 13, and July 21. Therefore,

Table I. Fractional water area and coefficients of second-order polynomial regression of log-transformed water areas against log-transformed exceedance probabilities for remotely sensed water areas at St. Denis Basin

Date	Total water area as percentage of basin area	Coefficients of second-order polynomial regression			
		c1 (intercept)	c2 (linear)	c3 (quadratic)	r^2
Apr. 13, 2011	4.4%	−0.781	0.990	−0.299	0.994
Apr. 30, 2011	11.9%	0.366	0.008	−0.080	0.995
May 13, 2011	7.5%	−0.125	0.341	−0.139	0.997
Jul. 21, 2011	4.5%	0.249	0.329	−0.220	0.997

DOI: 10.1002/hyp

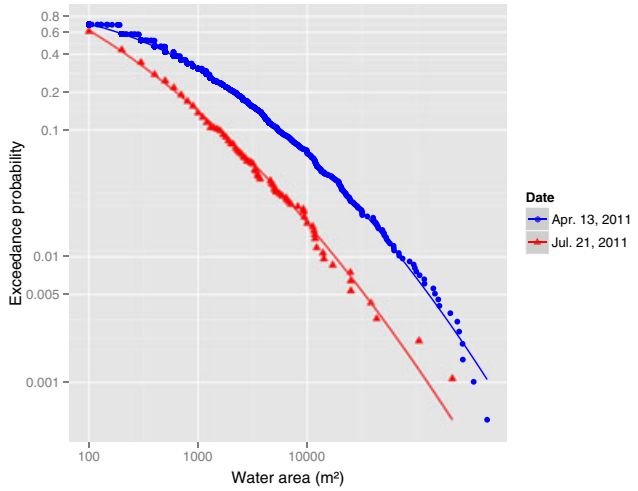

Figure 7. Logarithmic plot of exceedance probability *versus* area for water remotely sensed at St. Denis Basin on April 13, and July 21, 2011. The lines represent second-order polynomials fitted to the log-transformed probabilities and areas

neither the total area of open water, nor the areas of large water bodies can be used to characterize the state of storage in a prairie wetland complex, due to the existence of hysteresis.

It follows that the frequency distribution of open water areas uniquely defines the state of a wetland complex within a drainage basin at any given moment. Using the parameters of a second-order polynomial fitted to the log-transformed distribution, the open water area PDF, and therefore the state of the wetland complex, can be quantified. The three parameters of the polynomial are the state variables of the wetland complex.

Modelling water area frequency distributions at SCRB with the WDPM

Comparing the open water areas simulated by the WDPM with those determined by remote sensing is challenging because the model does not use realistic fluxes and so cannot calculate realistic water areas during partially filled conditions. However, the completely filled state is unique (only attainable by one set of state variables), allowing direct comparison between WDPM and remotely sensed data. In the spring of 2011, the wetlands at SCRB were very close to being completely filled.

Over the interval May 1, 2010 to April 30, 2011, 661.5 mm of precipitation was recorded at Yorkton, SK, which is the closest Environment Canada gauge, located approximately 60 km from SCRB. As the 1971–2000 annual normal precipitation at Yorkton is 450.9 mm, the interval was a very wet 12 months. On April 30, 2011, the Alter-shielded Geonor precipitation gauge operated by the Centre for Hydrology at SCRB recorded 28.5 mm water equivalent of snowfall. The rapid melt and subsequent runoff of this snowfall combined with accumulated precipitation, redistributed snow and runoff already stored in wetlands, to produce widespread flooding of agricultural land within the SCRB.

According to the Water Survey of Canada, provisional real-time data (available at http://www.wateroffice.ec.gc.ca/), the peak manual stage gauging at Smith Creek (station 05ME007), which also appears to be the peak discharge (19.7 m^3/s), was measured on May 4, 2011. The greatest recorded instantaneous discharge over the period of record (1975 to 2011) was 24.7 m^3/s in 1995. The reason for the apparent moderate response of Smith Creek to the very large runoff event of 2011 was that the discharge at the gauge was controlled by a culvert in an adjacent road. The road acted to dam the streamflow, causing the water to pond behind it forming a whirlpool over the Water Survey gauge and culvert and only exiting the basin via the restricted flow through the culvert. In 1995, the culvert and road were washed out, and so outflow was not restricted by culvert flow capacity. Over 2011, the total volume of flow was 66.9 million m^3 (computed from provisional data) which was more than double the previous maximum annual flow of 28 million m^3 in 1995.

The very wet conditions experienced at SCRB in the spring of 2011 resulted in wetland complexes reaching levels where the landscape was very close to being filled. The remotely sensed data were acquired on May 18, 2011 and presumably represent conditions slightly after the maximum extent of open water area in the basin. To simulate these conditions, WDPM was run for 75 sequences of inputs which included filling (water added to an initially empty basin), emptying (water removed from an initially filled basin) and alternating addition and removal of water. For each model run, second-order polynomials were fitted to the log-transformed open water areas and their frequencies to describe the frequency distribution of open water. The spaces occupied by the points in each of the plots are roughly triangular, showing the greatest ranges for values in the middle of the domains. This pattern is caused by hysteresis in the water area PDFs, which was demonstrated by the points describing loops as they were plotted against the fractional water area (although it is not visible in the plots). As described previously, the completely filled or completely emptied states are described by a single set of coefficients. As the set of wetlands approaches either state, the variability in its coefficients diminishes, regardless of whether it is filling or emptying.

None of the coefficients of the polynomials plotted in Figure 8 exactly match those of the remotely sensed data, although the remotely sensed coefficients clearly lie within the range occupied by the simulation coefficients. The WDPM simulation whose coefficients most closely resemble those of the remotely sensed data was based on an application of 400 mm of water, which is sufficient to fill all of the depressional storage, followed by the removal of 200 mm of water. The probability distributions of the WDPM simulation and the remotely sensed data are plotted in Figure 9. To compensate for the differing spatial resolutions of the RapidEye platform (5 m) and the WDPM (10 m), only open-water areas equal to or greater than 100 m^2 (the minimum area simulated by WDPM) are

DOI: 10.1002/hyp

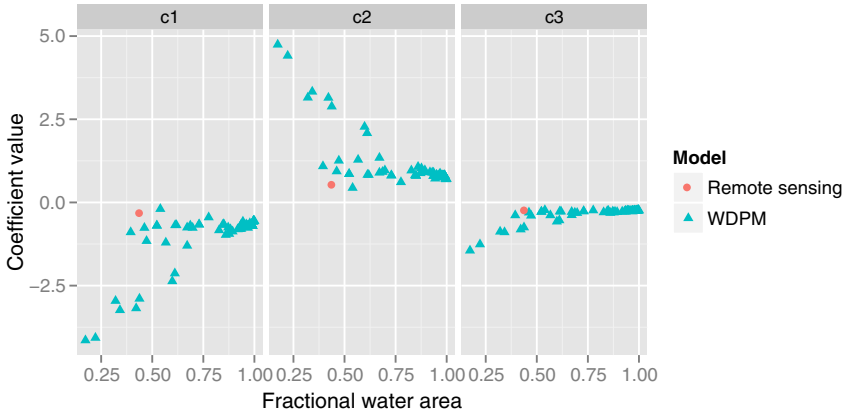

Figure 8. Plots of coefficients (c1 = intercept, c2 = linear, c3 = quadratic) of second order-polynomials fitted to the log-transformed probabilities and areas of remotely sensed data (May 18, 2011) and the WDPM simulations

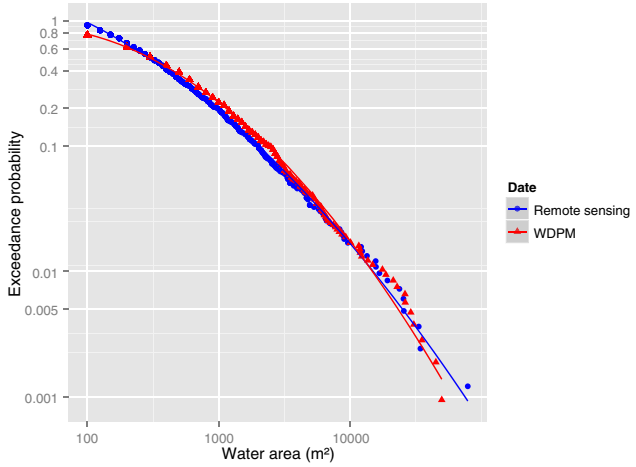

Figure 9. Logarithmic plot of exceedance probability *versus* area for water remotely sensed at the SCRB sub-basin 5 on May 18, 2011, and simulated by the WDPM. The lines represent second-order polynomials fitted to the log-transformed probabilities and areas. Only remotely sensed water areas greater than or equal to 100 m^2 (the minimum resolution of the LiDAR used by the WDPM) are plotted

plotted. The coefficients of second-order polynomials fitted to the log-transformed distributions are listed in Table II.

The sequence of events simulated by WDPM in this closest simulation to observations is believed to generally resemble the events which occurred at the SCRB before the acquisition of the remotely sensed data, in that the SCRB wetland complex was brought very close to being filled by the spring freshet, followed by loss of water by infiltration, drainage and evaporation. The actual mean depths of water applied to and removed from the SCRB are unknown, but a removal of 200 mm is not plausibly due to evaporation and infiltration over the 14 days which passed between the measured peak flow and the date of the remote sensing. However, Smith Creek basin has been subjected to extensive artificial drainage (Brunet and Westbrook, 2012) which undoubtedly increased the rate at which water was removed from the landscape. Artificial drainage is believed to be biased towards large wetlands, as very small wetlands are unlikely to be worth the expense of draining.

The spatial uniformity of the WDPM fluxes may also have contributed to the apparently large magnitude of the drainage required to fit the simulated storage states. WDPM does not incorporate the effects of wind redistribution (blowing snow transport and sublimation) on the spatial distribution of the winter snowpack, which may affect the frequency distribution of open water areas as snow is preferentially deposited in and near wetlands (Fang and Pomeroy, 2009). The WDPM also does not incorporate spatial variability in evaporation or infiltration, which have been shown to cause small wetlands to empty more rapidly than large ones (van der Kamp and Hayashi, 1998; Johnson *et al.*, 2010).

The differences between the methods used by the WDPM and the remote sensing image classifications to discriminate between water and water-free regions may also contribute to the very large simulated drainage. As described previously, the processes of image classification were very complex and were preformed with reference to photographs and ground truthing to obtain the best results possible. By contrast, the WDPM assigns array elements containing less than 1 mm of water to be water free, all other elements being designated as containing water. If the water areas simulated by the WDPM are consistently larger than the remotely sensed areas, then the model will require greater evaporation fluxes and smaller runoff fluxes to produce water areas similar to those of the remotely sensed images. Further research on this topic is warranted.

Despite the uncertainties in the measured and modelled fluxes, there is close agreement between the probability distributions of the remotely sensed open water areas and that of artificially filled/emptied/drained LiDAR DEM open water modelled by the WDPM. Therefore, it is asserted that the water redistribution mechanism of the WDPM is substantially correct.

Modelling water area frequency distributions at SDNWA with the WDPM

The performance of the WDPM was also tested by examining the changes in the open water area frequency distribution as water was added to and removed from

DOI: 10.1002/hyp

Table II. Fractional water area and coefficients of second-order polynomial regression of log-transformed water areas against log-transformed exceedance probabilities for remotely sensed and simulated water areas at SCRB

Method	Total water area as percentage of basin area	Coefficients of second-order polynomial regression			
		c1 (intercept)	c2 (linear)	c3 (quadratic)	r^2
Remote sensing	10.4%	−0.311	0.532	−0.234	0.996
WDPM	12.5%	−0.696	0.855	−0.280	0.998

wetlands. The sequence of the addition and removal of water was intended to mimic the behaviour of the wetlands at St. Denis Basin during the spring of 2011. Site visits indicate that runoff began in early April and that wetlands continued to drain throughout the period during which satellite imagery was acquired. Therefore, the wetlands experienced the typical Prairie spring additions of water from snow melt runoff, followed by removal of water due to evapotranspiration, infiltration and drainage. The depths of water added and subtracted were selected to cause the modelled fractional areas to be similar to those of the remotely sensed St. Denis Basin data for April 13, April 30 and May 13, 2011. No attempt was made to simulate the remotely sensed data of July 21, 2011 as by this date, the wetland complex had been subjected to an unknown sequence of additions and removals of water.

Figure 10 plots filling and emptying trajectories of the open water area probability distributions computed by the WDPM, using the SDNWA LiDAR data. Initially, 2 mm of water was added to the previously empty DEM. In the second iteration, a further 12 mm was then added for a total of 14 mm. Finally, a uniform depth of 75 mm was removed from the DEM. As the resolutions of the model and the remotely sensed images are very different, all analyses were restricted to wetland areas greater than 100 m^2 in area. As with the SCRB model, the modelled sequence of additions and removals of water are simplistic. The initial addition of only 2 mm indicates

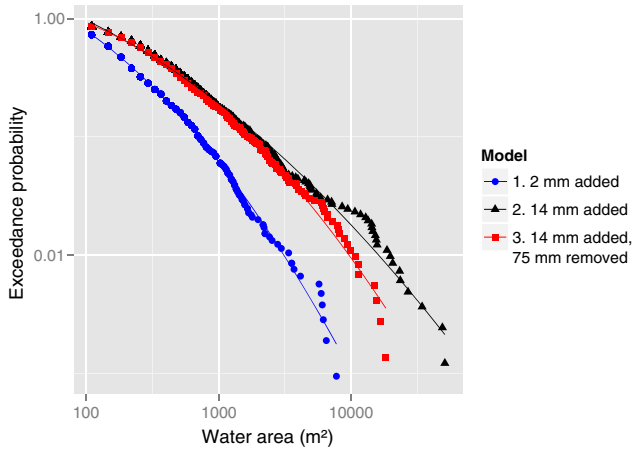

Figure 10. Logarithmic plot of exceedance probability *versus* area for water areas produced by the WDPM for the addition of 2 mm, 14 mm to, and the removal of 75 mm of water from, the LiDAR DEM for SDNWA. The lines represent second-order polynomials fitted to the log-transformed probabilities and areas

that the extent of the open water on April 13, 2011 was probably very similar to that when the LiDAR data were collected. The removal of 75 mm of water over the interval April 30–May 13 is not plausibly due to evapotranspiration alone, but losses may be additionally due to infiltration and drainage. As with the SCRB data, the differences in the differentiation of water/non-water regions between the classified remotely sensed data and the WDPM may also contribute to error in the applied flux. Additionally, the remotely sensed data are for the entire St. Denis Basin, while the modelled data are based on the LiDAR for the SDNWA.

The water area frequency distributions plotted in Figure 10 strongly resemble the remotely sensed distributions plotted in Figure 6. The modelled increased addition of water, from 2 mm to 14 mm, caused the open water area frequency distribution plot to pivot counter-clockwise. The removal of 75 mm water caused the plot to shift leftward, and rotate clockwise, as was seen in the remotely sensed St. Denis Basin data. The coefficients of the second-order polynomials fitted to the log-transformed open water area probability distributions listed in Table III, also strongly resemble those of the remotely sensed water areas.

The similarity of the modelled and remotely sensed open water area frequency distributions is taken to indicate that the spatial distribution algorithm of WDPM is generally sufficient for the purposes of this analysis. As the simulated probability distribution of open water areas changes in a similar way to the remotely sensed data, it is believed that the WDPM, if forced by realistic fluxes, could produce frequency distributions of open water area similar to those that would be observed. However, driving WDPM with realistic input and output fluxes remains problematic as previously discussed.

Parameterizing the PCM from the WDPM

The results indicate that WDPM redistributes water accurately; if the response of the conceptual PCM to simulated fluxes of water can be shown to be similar to that of the fully distributed WDPM, then it may be assumed that the response of the PCM to simulated fluxes can also be accurate. The PCM uses statistically representative models of wetlands to simulate the interconnections within wetland complexes. Shook and Pomeroy (2011) used the WDPM and an earlier version of the PCM to model the changes of contributing area of the SCRB sub-basin 5 in response to simulated fluxes of runoff and evaporation.

DOI: 10.1002/hyp

Table III. Water coverage and coefficients of second-order polynomial regression of log-transformed water areas against log-transformed exceedance probabilities for water areas greater than or equal to 100 m^2 remotely sensed at the St. Denis Basin and simulated by the WDPM at SDNWA

Method	Total water area as percentage of basin area	Coefficients of second-order polynomial regression			
		c1 (intercept)	c2 (linear)	c3 (quadratic)	r^2
Remote sensing					
Apr. 13, 2011	4.4%	−0.319	0.545	−0.330	0.999
Apr. 30, 2011	11.9%	0.106	0.119	−0.164	0.995
May 13, 2011	7.5%	−0.491	0.638	−0.271	0.997
WDPM Model					
2 mm applied	4.9%	−0.386	0.426	−0.156	0.998
14 mm applied	11.7%	0.021	0.135	−0.096	0.993
75 mm removed	6.7%	−0.524	0.664	−0.276	0.996

The minimum number of wetlands used, and their connectivity, was derived from the relative frequencies of wetlands present at each Horton–Strahler level of an imposed drainage network. The Horton–Strahler levels are assigned to stream segments based on the order of their connectivity (Strahler, 1957). For the SCRB sub-basin 5, at least 46 wetlands were required to adequately represent connectivity in PCM (Shook and Pomeroy, 2011). Although the PCM with 46 wetlands was also partially able to reproduce the changes in contributing area caused by changes in the volume of water stored in the basin, it invariably underestimated the contributing area, compared to the WDPM. Use of multiple sets of 46 wetlands improved the representation of contributing area, but the problem was not eliminated and model complexity increased substantially.

Further analysis shows that the underestimation of the basin-scale contributing area by the PCM appears to be caused by the method of estimating the contributing areas of the individual modelled wetlands. The wetland drainage area is the area which can drain to a given wetland, including the wetted area and the upland area which can potentially contribute runoff to the wetland.

In the absence of any published information or field studies, it was previously assumed (incorrectly) by Shook and Pomeroy (2011) that the ratio of wetland drainage area to maximum wetland area would be fairly constant for all wetlands. Here, using a modified version of the WDPM, the drainage area was found for each wetland by (1) filling the DEM to its maximum extent, (2) tracing the flow path from each non-wetted cell in the DEM to its termination in a water body and (3) counting the number of cells (wetted and non-wetted) which contribute to each water body. As the SDNWA does not drain to a stream, it was not possible to completely fill and drain the landscape. In this case, the same depth of water added to the other basins (400 mm) was added to SDNWA.

The calculations were carried out using LiDAR DEM data at Vermillion River Basin, the SDNWA and the SCRB. Figure 11 plots the contributing area against wetland area for all three sites. Although the plots display a great degree of scatter for the smaller values, all three sites showed scaling relationships between open water area and basin area. Surprisingly, the scaling relationships were all very similar: the exponents of least-squares fitted power-law relationships, for the SCRB, SDNWA and Vermillion River basin plots are 0.717, 0.704 and 0.746, respectively. As the exponents are smaller than 1.0, the total drainage area increases more slowly than does the maximum open water area. This means that the upland drainage area increases more slowly than does the wetland area and so larger wetlands will tend to have contributing areas which are smaller fractions of their maximum water areas, than will smaller wetlands.

Non-integer scaling relationships are common with collections of fractal objects (Mandelbrot, 1982; Shook

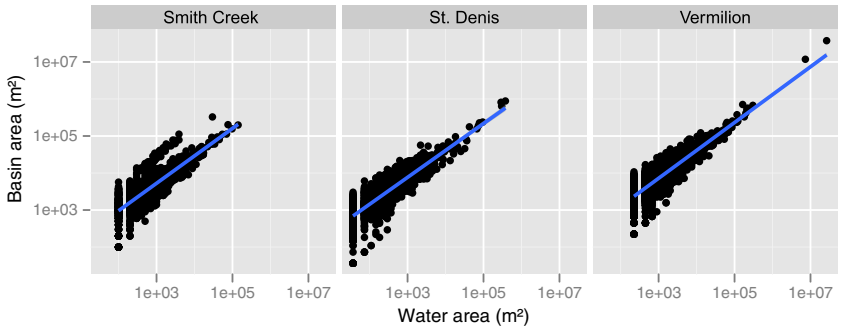

Figure 11. Logarithmic plots of basin area *versus* maximum water area for wetlands in the LiDAR coverage of the Vermilion, SDNWA, and SCRB basins

DOI: 10.1002/hyp

et al., 1993). Prairie wetlands show fractal-type scaling in their perimeter length (Minke *et al.*, 2010). Sets of fractal objects, such as lakes or islands, generally fit non-integer power-law distributions (Mandelbrot, 1982), which is approximately true of wetland open water areas. Therefore, the existence of non-integer scaling relationships between maximum wetland open water area and basin area might have been expected. As a test of the scale(s) over which the scaling is valid, areas of lakes and their basins were obtained for Alberta from Mitchell and Prepas (1990), and for Saskatchewan, Manitoba and North Dakota from van der Kamp *et al.* (2008) and are plotted in Figure 12. The examined lakes have similar power-law basin scaling relationships to those of the wetlands. The greater value of the scaling exponent of the lake basins (0.90) than for the wetland basins is believed to be due to the lakes not filling their basins to the fill and spill sill levels, resulting in smaller open water areas relative to the basin areas.

For wetlands having areas greater than 1000 m^2, the PCM was revised to include the observed non-integer basin scaling to specify the area contributing to each wetland, Because of the large scatter shown in Figure 11 for small wetlands, those wetlands having maximum areas equal to or smaller than 1000 m^2 had basin areas arbitrarily set to the mean value for wetlands in their size class. When forced by simplified fluxes, both the PCM, with 16 sets of 46 wetlands to parameterize fully distributed wetlands, and the WDPM produced similar hysteretic plots of contributing area *versus* depressional storage, as shown in Figure 13. As water was added, the contributing area increased until the entire sub-basin contributed. The initial removal of water resulted in rapid reduction of contributing area to near zero. Further removal of water reduced the volume of water stored in the basin whilst keeping the fraction of area contributing at zero.

Incorporating the PCM in a hydrological model will be less computationally expensive if smaller numbers of wetlands can be modelled. Figure 14 plots the contributing area modelled by the PCM using 1, 2, 4, 8 and 16 sets of 46 simulated wetlands. Note that only the rising limbs (i.e. due to the addition of water) are plotted, as the falling limbs (due to the removal of water) are all identical. The plots indicate that using smaller numbers of wetlands cause the plots to zig-zag, rather than describing a fairly smooth curve, probably due to the 'gatekeeper' effect identified by Phillips *et al.* (2011), where a few large downstream wetlands prevent all upstream land from contributing until they are filled. Using smaller numbers of wetlands in the simulation exaggerated the importance of individual large wetlands, causing an apparent 'staircase' effect that is not observed in nature for wetland systems in the prairie environment.

However, the plots show that, overall, the number of sets of wetlands used did not strongly affect the fractional

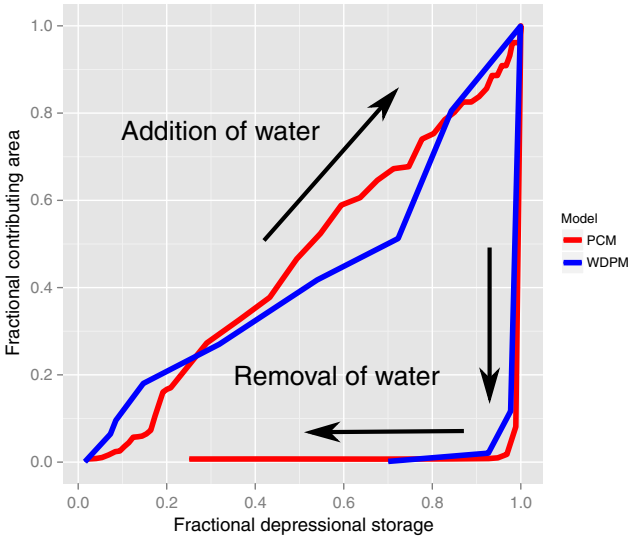

Figure 13. Fractional contributing area *versus* fractional depressional storage for the WDPM and the PCM. In both cases, water was added iteratively, up to a total of 400 mm. This was followed by removing water

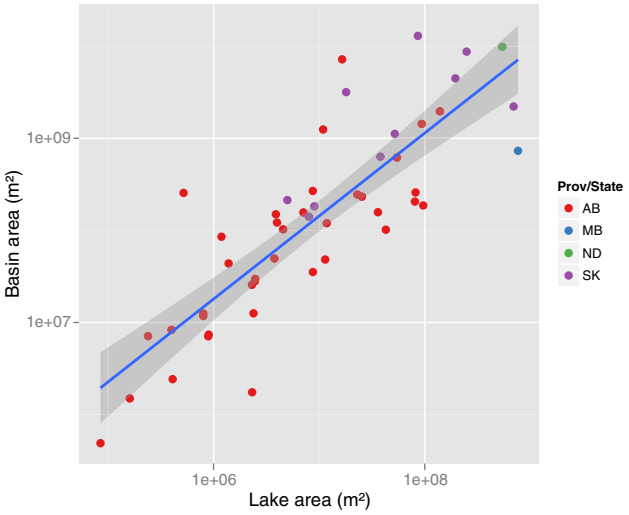

Figure 12. Logarithmic plots of basin area *versus* area for lakes in Alberta, Saskatchewan, Manitoba and North Dakota

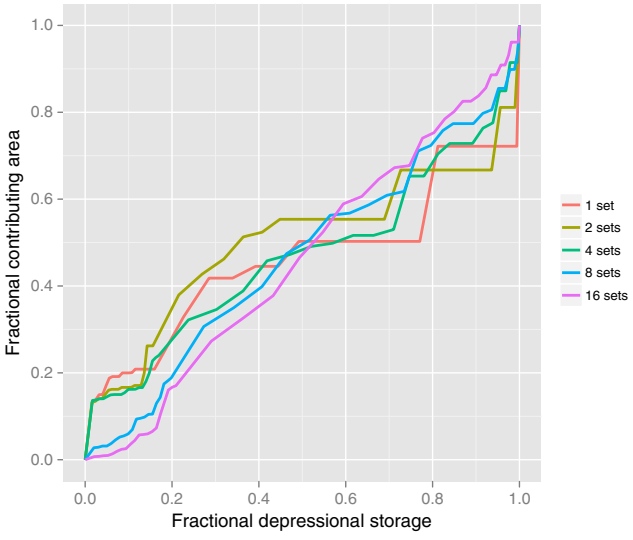

Figure 14. Curves of fractional contributing area *versus* fractional depressional storage for the PCM using 1, 2, 4, 8 and 16 sets of 46 wetlands

DOI: 10.1002/hyp

contributing area computed by the PCM, and that even relatively small numbers of simulated wetlands, when used with accurate basin areas, can be used to simulate the hysteretic behaviour of a wetland complex. This is an important parameterization for conceptual models of Prairie wetland basins storage dynamics that will be suitable for application at medium to large scales.

SUMMARY AND CONCLUSIONS

This research has advanced toward the goal of physically based modelling of the hydrology of prairie wetland complexes, by partially validating a fully distributed and a parameterized model of wetland storage dynamics and contributing area.

Remotely sensed measurements show that the frequency distribution of wetland open water areas characterizes the state of wetlands in a basin. Although the open water area probability frequency distributions deviate from the ideal power-law distribution, the actual distributions can be characterized by a second-order polynomial fitted to the log-transformed frequency distribution. The sets of coefficients of the polynomials can be used to characterize open water area probability distributions and can therefore be regarded as being a state variable.

Although it is currently forced with very simplified fluxes of water, the fully distributed wetland dynamics model was able to produce probability distributions of open water areas which were very similar to those obtained by remote sensing of open water areas in post-flooding conditions. When parameterized using relations between wetland drainage area and wetland area from the fully distributed model, the parameterized wetland storage and contributing area model was able to produce a hysteresis loop very similar to that produced by the distributed model for the same input and output fluxes.

The ultimate goal of the parameterized PCM is to incorporate it in physically based models of prairie hydrology. However, the PCM cannot currently produce the same frequency distributions of open water areas as the distributed model for states where the wetlands are less than full. Consequently, the PCM cannot be initialized and hence not verified against remotely sensed data. It may be possible to initialize PCM by spinning it up, if the model can be shown to reach an equilibrium state regardless of the initial state, for a sufficiently long set of modelled fluxes. Further research is required to fully implement PCM in a hydrological model, and the final verification of its usefulness will be whether it can improve dynamical contributing area and streamflow calculations in hydrological models applications in the prairie environment.

ACKNOWLEDGEMENTS

The authors wish to thank Michael Barr, North Saskatchewan Watershed Alliance for the Vermilion LiDAR data; the Governments of Saskatchewan and Manitoba for the Smith Creek LiDAR data; and Ducks Unlimited Canada, for the RapidEye data obtained from Blackbridge Geomatics. Financial support from CRC, NSERC, DUC and the U of S Global Institute for Water Security is gratefully acknowledged. Computational support was provided by the WestGrid research consortium.

This research was done entirely with Free Open Source Software. All maps were created using Quantum GIS (http://www.qgis.org/). All graphs were plotted in R, using the package ggplot2 (Wickham, 2009).

REFERENCES

Armstrong RN, Pomeroy JW, Martz LW. 2008. Evaluation of three evaporation estimation methods in a Canadian prairie landscape. *Hydrological Processes* **22**(May): 2801–2815. DOI: 10.1002/hyp. 7054.

Brunet NN, Westbrook CJ. 2012. Wetland drainage in the Canadian prairies: Nutrient, salt and bacteria characteristics, Agriculture. *Ecosystems & Environment* **146**(1): 1–12. DOI: 10.1016/j.agee.2011.09.010.

Christiansen EA. 1979. The Wisconsinan deglaciation of southern Saskatchewan and adjacent areas. *Canadian Journal of Earth Sciences* **16**: 913–938.

Coles S. 2001. *An introduction to statistical modeling of extreme values*. Springer-Verlag: London.

Congalton RG. 1991. A Review of Assessing the Accuracy of Classifications of Remotely Sensed Data. *Remote Sensing of Environment* **37**: 35–46.

Driver EA, Peden DG. 1977. The Chemistry of Surface Water in Prairie Ponds. *Hydrobiologia* **53**(1): 33–48.

Elliott JA, Efetha AA. 1999. Influence of tillage and cropping system on soil organic matter, structure and infiltration in a rolling landscape. *Canadian Journal of Soil Science* **79**: 457–463.

Fang X, Pomeroy JW. 2007. Snowmelt runoff sensitivity analysis to drought on the Canadian prairies. *Hydrological Processes* **2609**(19): 2594–2609. DOI: 10.1002/hyp.

Fang X, Pomeroy JW. 2008. Drought impacts on Canadian prairie wetland snow hydrology. *Hydrological Processes* **22**(15): 2858–2873. DOI: 10.1002/hyp.7074.

Fang X, Pomeroy JW. 2009. Modelling blowing snow redistribution to prairie wetlands. *Hydrological Processes* **23**(18): 2557–2569. DOI: 10.1002/hyp.7348.

Fang X, Pomeroy JW, Westbrook CJ, Guo X, Minke AG, Brown T. 2010. Prediction of snowmelt derived streamflow in a wetland dominated prairie basin. *Hydrology and Earth System Sciences* **14**(6): 991–1006. DOI: 10.5194/hess-14-991-2010.

Förster M, Schuster C, Kleinschmit B. 2010. Significance analysis of multi-temporal RapidEye satellite images in a land-cover classification, in Accuracy 2010 Symposium, July 20-23, edited by Tate NJ, Fisher PF (eds), pp. 273–276, Leicester, UK.

Garbrecht J, Martz LW. 1997. The assignment of drainage direction over flat surfaces in raster digital elevation models. *Journal of Hydrology* **193**(1-4): 204–213. DOI: 10.1016/S0022-1694(96)03138-1.

Godwin RB, Martin FRJ. 1975. Calculation of gross and effective drainage areas for the Prairie Provinces. In: Canadian Hydrology Symposium - 1975 Proceedings, 11-14 August 1975, Winnipeg, Manitoba. Associate Committee on Hydrology, National Research Council of Canada, pp. 219–223.

Granger RJ, Hedstrom N. 2011. Modelling hourly rates of evaporation from small lakes, *Hydrology and Earth System Sciences* **15**(1): 267–277. DOI: 10.5194/hess-15-267-2011.

Gray DM. 1964. Physiographic Characteristics and the Runoff Pattern, in Proceedings of Hydrology Symposium No. 4 Research Watersheds, pp. 146–164, National Research Council of Canada Associate Committee on Geodesy and Geophysics Subcommittee on Hydrology.

Gray DM, Pomeroy JW, Granger RJ. 1986. Prairie snowmelt runoff. In *Proceedings, Water Research Themes, Conference Commemorating the Official Opening of the National Hydrology Research Centre*. Canadian Water Resources Association, Saskatoon, 49–68.

Gray DM, Pomeroy JW, Granger RJ. 1989. Modelling snow transport, snowmelt and meltwater infiltration in open, northern regions. In *Northern Lakes and Rivers*, Occasional Publication No. 22, Mackay WC (ed). Boreal Institute for Northern Studies, Univ. of Alberta: Edmonton; 8–22.

Hayashi M, van der Kamp G. 2000. Simple equations to represent the volume-area-depth relations of shallow wetlands in small topographic depressions. *Journal of Hydrology* **237**: 74–85.

Hayashi M, van der Kamp G, Rudolph DL. 1998. Water and solute transfer between a prairie wetland and adjacent uplands, 1. Water balance. *Journal of Hydrology* **207**: 42–55.

Hayashi M, van der Kamp G, Schmidt R. 2003. Focused infiltration of snowmelt water in partially frozen soil under small depressions. *Journal of Hydrology* **270**: 214–229.

Johnson WC, Werner B, Guntenspergen GR, Voldseth RA, Millett B, Naugle DE, Tulbure M, Carroll RWH, Tracy J, Olawsky C. 2010. Prairie Wetland Complexes as Landscape Functional Units in a Changing Climate. *BioScience* **60**(2): 128–140. DOI: 10.1525/bio.2010.60.2.7.

van der Kamp G, Hayashi M. 1998. The Groundwater Recharge Function of Small Wetlands in the Semi-Arid Northern Prairies. *Great Plains Research* **8**: 39–56.

van der Kamp G, Hayashi M, Gallen D. 2003. Comparing the hydrology of grassed and cultivated catchments in the semi-arid Canadian prairies. *Hydrological Processes* **575**(September 2001): 559–575. DOI: 10.1002/hyp.1157.

van der Kamp G, Keir D, Evans MS. 2008. Long-Term Water Level Changes in Closed-Basin Lakes of the Canadian Prairies. *Canadian Water Resources Journal* **33**(1): 23–38.

Kuchment LS, Gelfan AN, Demidov VN. 2000. A distributed model of runoff generation in the permafrost regions. *Journal of Hydrology* **240**: 1–22.

Lidar Services International. 2009. Manitoba Water Stewardship and Saskatchewan Water Authority October 2008 LiDAR Survey Report.

Lillesand T, Kiefer R, Chipman J. 2004. *Remote sensing and image interpretation*. John Wiley & Sons, Inc: New York.

Mandelbrot B. 1982. *The Fractal Geometry of Nature*. W. H. Freeman and Company: New York, New York, USA.

Marshall IB, Scott Smith CA, Selby CJ. 1996. A National Framework For Monitoring And Reporting On Environmental Sustainability in Canada. *Environmental Monitoring and Assessment* **39**: 25–38.

Mekonnen MA, Davison B, Toth B, Liu A, Pietroniro A, Pomeroy J, Macdonald MK, Ireson A. n.d. An atmospheric-hydrologic-land surface modelling platform for the South Saskatchewan River Basin, Submitted to Hydrology Research.

Miller JJ, Acton DF, Arnaud RJST. 1985. The Effect of Groundwater on Soil Formation in a Morainal Landscape in Saskatchewan. *Canadian Journal of Soil Science* **65**: 293–307.

Minke AG, Westbrook CJ, van der Kamp G. 2010. Simplified Volume-Area-Depth Method for Estimating Water Storage of Prairie Potholes. *Wetlands* **30**(3): 541–551. DOI: 10.1007/s13157-010-0044-8.

Mitchell P, Prepas E (eds). 1990. Atlas of Alberta lakes, University of Alberta Press, Edmonton, Alberta. Available from: http://sunsite.ualberta.ca/Projects/Alberta-Lakes/.

Oswald CJ, Richardson MC, Branfireun BA. 2011. Water storage dynamics and runoff response of a boreal Shield headwater catchment. *Hydrological Processes* **25**: 3042–3060. DOI: 10.1002/hyp.8036.

Phillips RW, Spence C, Pomeroy JW. 2011. Connectivity and runoff dynamics in heterogeneous basins. *Hydrological Processes* **3075**(May): 3061–3075. DOI: 10.1002/hyp.8123.

Pomeroy JW, Gray DM, Landine PG. 1993. The Prairie Blowing Snow Model: characteristics, validation, operation. *Journal of Hydrology* **144**(1-4): 165–192. DOI: 10.1016/0022-1694(93)90171-5.

Pomeroy JW, Gray DM, Brown T, Hedstrom NR, Quinton WL, Granger RJ, Carey SK. 2007a. The cold regions hydrological model: a platform for basing process representation and model structure on physical evidence. *Hydrological Processes* **21**(19): 2650–2667. DOI: 10.1002/hyp.6787.

Pomeroy JW, de Boer D, Martz LW. 2007b. Hydrology and Water Resources. In *Saskatchewan: Geographic Perspectives*, Thraves B, Lewry M, Dale J, Schlichtmann H (eds). Canadian Plains Research Centre: Saskatoon, Saskatchewan; 63–80.

Pomeroy J, Fang X, Westbrook C, Minke A, Guo X, Brown T. 2010. Prairie Hydrological Model Study Final Report. Centre for Hydrology Report No. 7, University of Saskatchewan, Saskatoon, Saskatchewan.

Pomeroy JW, Fang X, Shook K, Westbrook C, Brown T. 2012. Informing the Vermilion River Watershed Plan through Application of the Cold Regions Hydrological Model Platform. Centre for Hydrology Report No. 12, University of Saskatchewan, Saskatoon, Saskatchewan.

R Development Core Team. 2011. R: A language and environment for statistical computing, R Foundation for Statistical Computing, Vienna, Austria. Available from: http://www.r-project.org/.

Ricci V. 2005. Fitting distributions with R, Foundation for Statistical Computing, Vienna, Austria. Available from: http://www.r-project.org/.

Seekell DA, Pace ML. 2011. Does the Pareto distribution adequately describe the size-distribution of lakes? *Limnology and Oceanography* **56**(1): 350–356. DOI: 10.4319/lo.2011.56.1.0350.

Shapiro M, Westervelt J. 1992. An Algebra for GIS and Image Processing. U.S.Army Corps of Engineers, Construction Engineering Research Laboratories, Champaign, Illinois, 422–425.

Shaw DA. 2009. The influence of contributing area on the hydrology of the prairie pothole region of North America, 169 pp., University of Saskatchewan.

Shaw DA, van der Kamp G, Conly FM, Pietroniro A, Martz L. 2011. The Fill – Spill Hydrology of Prairie Wetland Complexes during Drought and Deluge. *Hydrological Processes*. DOI: 10.1002/hyp.

Shook KR, Pomeroy JW. 2011. Memory effects of depressional storage in Northern Prairie hydrology. *Hydrological Processes* **25**(November): 3890–3898. DOI: 10.1002/hyp.8381.

Shook K, Pomeroy J. 2012. Changes in the hydrological character of rainfall on the Canadian prairies. *Hydrological Processes* **26**(12): 1752–1766. DOI: 10.1002/hyp.9383.

Shook KR, Gray DM, Pomeroy JW. 1993. Temporal Variation in Snowcover Area During Melt in Prairie and Alpine Environments. *Nordic Hydrology* **24**(1993): 183–198.

Spence C. 2007. On the relation between dynamic storage and runoff: A discussion on thresholds, efficiency, and function. *Water Resources Research* **43**(12): 1–11. DOI: 10.1029/2006WR005645.

Spence C, Woo M. 2003. Hydrology of subarctic Canadian shield: soil-filled valleys. *Journal of Hydrology* **279**(1-4): 151–166. DOI: 10.1016/S0022-1694(03)00175-6.

Spence C, Guan XJ, Phillips R, Hedstrom N, Granger R, Reid B. 2010. Storage dynamics and streamflow in a catchment with a variable contributing area. *Hydrological Processes* **24**: 2209–2221. DOI: 10.1002/hyp.7492.

Stichling W, Blackwell SR. 1957. Drainage area as an Hydrologic Factor on the Canadian Prairies, in IUGG Proceedings, Volume **111**, pp. 365–376.

Strahler AN. 1957. Quantitative Analysis of Watershed Geomorphology. *Transations of the American Geophysical Union* **38**(6): 913–920.

Töyrä J. 2005. Metadata for Preliminary LiDAR DEM-St. Denis NWA. National Water Research Institute, Environment Canada: Saskatoon, Canada, 5.

Tromp-van Meerveld HJ, McDonnell JJ. 2006. Threshold relations in subsurface stormflow: 2. The fill and spill hypothesis. *Water Resources Research* **42**(2): 1–11. DOI: 10.1029/2004WR003800.

Wickham H. 2009. *ggplot2: Elegant Graphics for Data Analysis*. Springer: New York.

Xu H. 2006. Modification of normalized difference water index to enhance open water features in remotely sensed imagery. *International Journal of Remote Sensing* **14**: 3025–3033.

Zhang B, Schwartz FW, Liu G. 2009. Systematics in the size structure of prairie pothole lakes through drought and deluge. *Water Resources Research* **45**(4): 1–12. DOI: 10.1029/2008WR006878.